Supporting information

Dynamics of Photoconversion Processes: Energetic Cost of Charge Separation in Photocatalysis and Photovoltaics

Robert Godin*[a,b,c] and James R. Durrant[b]

[a.] Department of Chemistry, The University of British Columbia, 3247 University Way, Kelowna, British Columbia, V1V 1V7, Canada
[b.] Clean Energy Research Center, University of British Columbia, 2360 East Mall, Vancouver, British Columbia, V6T 1Z3, Canada
[c.] Okanagan Institute for Biodiversity, Resilience, and Ecosystem Services, University of British Columbia, Kelowna, British Columbia, Canada
[d.] Department of Chemistry and Centre for Processable Electronics, Imperial College London, Exhibition Road, London SW7 2AZ, UK

Contents

Supporting information

Section S1. Details of kinetic competition and equilibrium

Taking the case where the rate of recombination from the charge separated state can be ignored and the reactions kinetics are first order, charge separation (CS) can be mainly considered as a simple equilibrium between two excited state energy levels (Scheme 2 of main text). The equilibrium satisfies:

$$K_{CS} = \frac{k_{CS}}{k_{-CS}} = \exp\left(-\frac{\Delta G_{CS}}{k_B T}\right)$$

Equation S1

The charge separation yield will be the fraction of the population found in the low energy state and is given by:

$$\Phi_{CS} = \frac{k_{forward}}{k_{forward} + \Sigma k_{backward}} = \frac{k_{CS}}{k_{CS} + k_{-CS}} = \frac{1}{1 + K_{CS}^{-1}}$$

Equation S2

Figure S1 shows how the yield depends on K_{CS}. The result is intuitive: a faster charge separation or longer charge separated lifetime (i.e., larger K_{CS} or smaller K_{CS}^{-1}) leads to a higher charge separation yield. To achieve > 90% yield, the forward rate of reaction needs to be at least a factor of 10 faster than the competing rates.
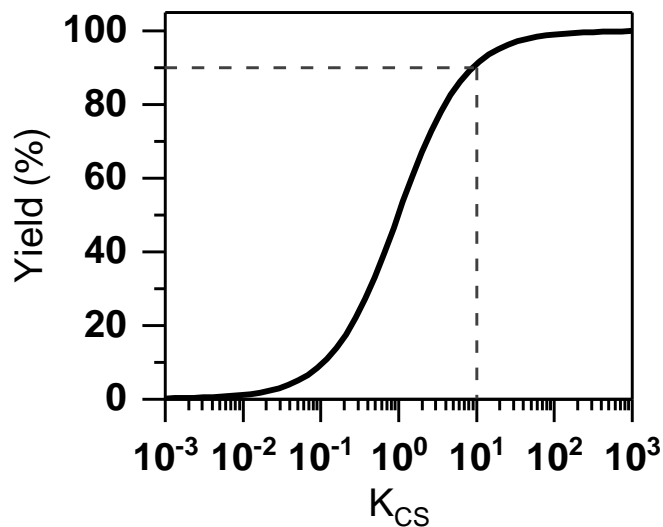

Figure S1. Plot showing the variation in charge separated yield for different ratios of rate constants. The dotted lines indicate that 90% yield is achieved for $K_{CS}^{-1} = 0.1$, that is K_{CS} = 10.

Following Equation S1, we see that the forward (k_{CS}) and backward (k_{-CS}) rates constants are linked through the equilibrium constant K_{CS}. In turn, the equilibrium constant is determined by the free energy difference (ΔG_{CS}) between the two states. For each increase in order of magnitude in K_{CS}, also corresponding to an order of magnitude increase in the ratio of the lifetime of the charge separated state ($\tau_{deact} = 1/k_{-CS}$) to its formation lifetime ($\tau_{CS} = 1/k_{CS}$), ΔG_{CS} becomes more favourable (i.e. more negative) by 59 meV at room temperature. There is clearly a trade-off between increasing the yield of charge separation and conserving the energy absorbed. The result is that there is a value of K_{CS} that maximizes energy conversion, as shown in Figure S2. Increasing K_{CS} past the optimal value results in a decrease of the energy converted due to the increasing energetic loss driving the forward step without additional gains in yield. Note that the optimal value of K_{CS} becomes larger for increasing values of energy input (see Figure S3).
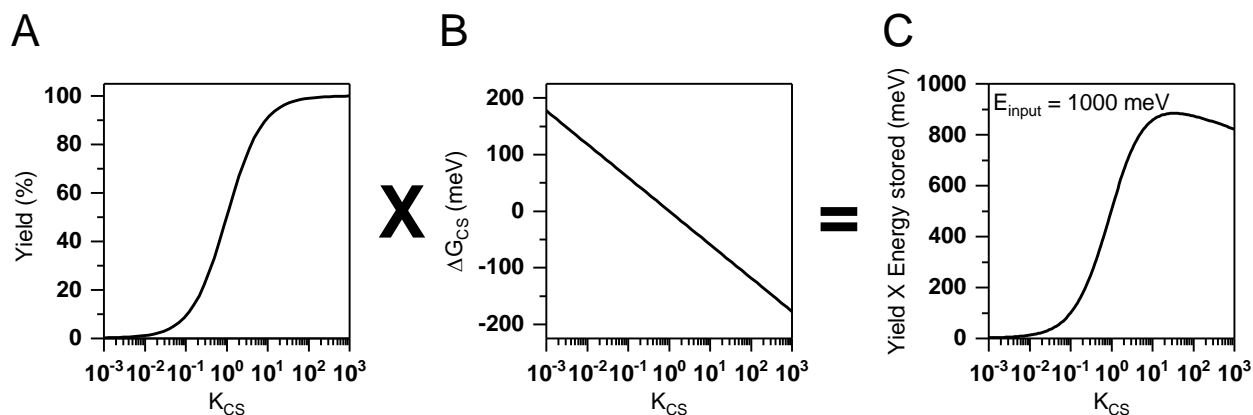
A   B   C

Figure S2. Link between the charge separation yield and energetics. A) Variation of yield with K_{CS}. B) Variation of ΔG_{CS} with K_{CS}. C) Variation of the overall conversion yield with K_{CS} using an example energy input of 1000 meV. This is obtained by multiplying the yield (panel A) and the energy stored (given from panel B and considering the energy input).
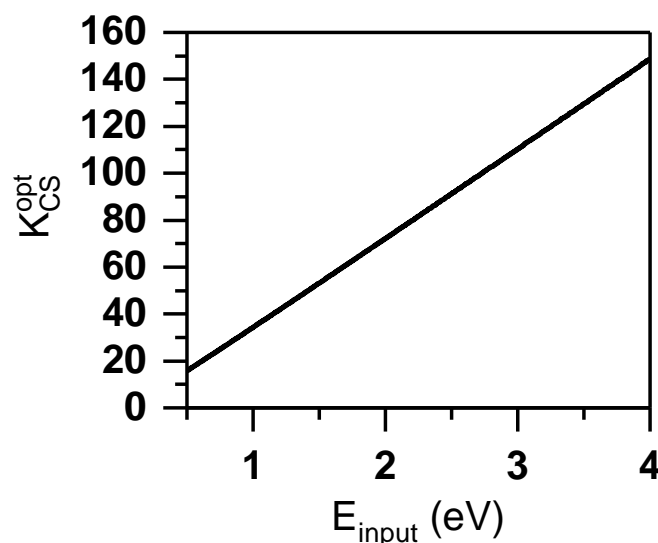

Figure S3. Variation of the optimal value of K_{CS} which maximizes overall energy conversion as a function of the energy input.

Devices under operation will assuredly have some active recombination pathways. Including this effect and keeping the simple first order kinetics, the yield of the charge separation step can be written in a form similar to Equation S2:

$$\Phi_{CS} = \frac{k_{CS}}{k_{CS} + k_{-CS} + k_r'} = \frac{1}{1 + \frac{k_{-CS} + k_r'}{k_{CS}}} = \frac{1}{1 + \frac{\tau_{CS}}{\tau_{deact}}}$$

Equation S3

τ_{deact}, the lifetime of the charge separated state, now includes the contribution from the recombination pathway (τ_{deact} = $1/[k_{-CS} + k_r']$). The yield for other steps shown in Scheme 1 of the main text are written in the same fashion, substituting for the appropriate rate constants or lifetimes. Keeping the example of the charge separation step, the dependence of the yield on the ratio τ_{CS}/τ_{deact} is shown in Figure S4 – this is the same situation as the simple case without recombination. As before, a faster charge separation or longer charge separated lifetime (now more easily seen as a smaller τ_{CS}/τ_{deact}) leads to a higher charge separation yield.
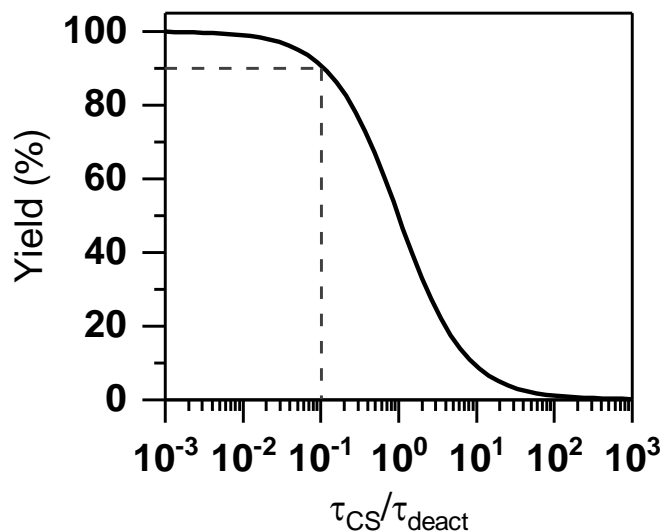
Figure S4. Dependence of the charge separation yield on the ratio of the lifetimes of the charge separation and the charge separated state.

By rewriting Equation S3 to clearly separate the rate constant ratios of $k_{-CS}/k_{CS} = K_{CS}^{-1}$ and k_r'/k_{CS}, we obtain:

$$\Phi_{CS} = \frac{1}{1 + \dfrac{k_{-CS}}{k_{CS}} + \dfrac{k_r'}{k_{CS}}}$$

Equation S4

Using the link between K_{CS} and ΔG_{CS} from Equation S1, we show the influence of the different rate constant ratios in Figure S5. Smaller values of the ratios k_{-CS}/k_{CS} and k_r'/k_{CS} lead to increase charge separation. The effect of the recombination pathway becomes negligible as k_r'/k_{CS} approaches 10^{-3}. A faster rate of forward charge separation (k_{CS}) is beneficial for the yield, yet it is critical to understand the mechanism of the increase in k_{CS}. If an increase is due to an increase in thermodynamic driving force, the overall energy conversion may suffer. Increasing k_{CS} through other means (e.g., optimizing molecular orientation, improving electronic coupling, reducing distance between charge transfer partners) or decreasing the rate constants of undesired processes (e.g., k_{-CS}, k_r) will often be a more productive path toward overall system optimization.
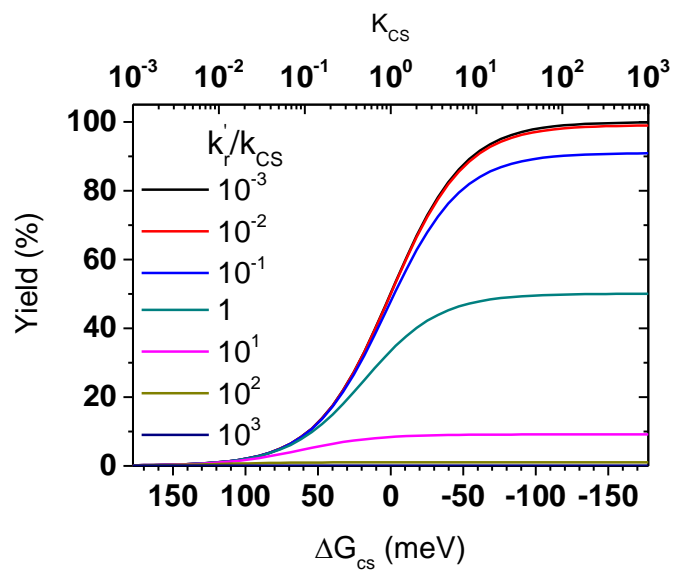
Figure S5. Plot showing the effect of the charge separation driving force on the yield of charge separation. Different ratios of charge recombination to charge separation rate constants are shown in different coloured lines.

Supporting information

Section S2. Considerations for charge carrier dynamics and energetic losses

S2.1 Charge separation.

Following absorption of a photon, the initial excited state is a bound electron-hole pair, termed exciton. The Coulombic attraction between the charges of opposite sign creates an energetic barrier to charge separation. We can define the Coulomb capture radius (R_c), the distance where the Coulomb energy is equal to the thermal energy:

$$R_c = \frac{e^2}{4\pi\varepsilon_0\varepsilon_r k_B T}$$

Equation S5

e is the elementary charge, ε_0 is the vacuum permittivity, ε_r is the dielectric constant of the medium, k_B the Boltzmann constant and T is the temperature.

At room temperature, the Coulomb capture radius is typically on the order of a few nanometres. The close proximity of the electron and hole makes charge recombination a very fast process, typically on the order of picoseconds – nanoseconds.[1] Recombination of photogenerated charges that originate from the same photon absorption process is termed 'geminate'. As a result, effective charge separation must be faster than geminate recombination, on sub-nanosecond timescales.

Depending on the class of solar energy conversion device, different approaches are taken to ensure a fast and efficient charge separation. Often, such as for organic bulk heterojunction (BHJ) solar cells and DSSCs, a considerable energy offset is used to drive rapid charge separation, incurring a large energetic cost. In inorganic semiconductors, such as Si or GaAs, a p-n junction spontaneously generates an interfacial electric field that adjusts the positions of the CB and VB in the p- and n-doped domains, providing the energetic driving force for charge separation. An applied bias is typically used in photoelectrodes to increase the band bending at the semiconductor/electrolyte interface and widen the associated space charge layer (SCL). The electric field within the SCL drives charges in opposite directions. In addition, spatial separation of charges has been shown to be an effective mechanism to reduce the rate of recombination and increase the yield of available charges.[2-6] However, as discussed above for natural photosynthesis, this typically requires multiple charge transfer steps, each associated with a loss of energy and complicates device fabrication.

S2.2 Charge transport

Once electron and hole have been separated, they must travel to their respective interfaces where extraction takes place. In the absence of an extracting electric field, the timescale of charge transport (t_{trans}) will depend on the distance to the interface (r) and the diffusion coefficient (D). For a 3D system, the diffusion equation becomes:

$$t_{trans} = \frac{\langle r^2 \rangle}{6D}$$

Equation S6

The diffusion coefficient is related to the charge mobility μ by the Einstein-Smoluchowski equation:

$$\mu = \frac{eD}{k_B T}$$

Equation S7

We thus obtain a relation between the charge transport time and charge mobility of $t_{trans} \propto 1/\mu$, or $k_{trans} \propto \mu$. Generally, a high mobility favours rapid charge extraction, although the exact relationship is more complex and can depend on physical characteristics such as the domain size in OPV blends.[7] Charge mobility itself is affected by many factors, such as the nature of the material, disorder, the charge carrier density, and impurities.[8]

At the same time, charge recombination will be a competing process leading to energy loss. In this case, the recombination is non-geminate in nature as charges originating from different charge carrier pairs may encounter each other. Furthermore, the rate of recombination depends on the concentration of both electrons and holes, leading to bimolecular behaviour.

Bimolecular recombination has been explained by many different physical models, as presented in Figure S6. *A priori*, an electron and hole will recombine when they come within R_c of each other, as described by Langevin theory.[9] When

the photogenerated charge carrier density is large compared to the intrinsic charge carrier density, the Langevin recombination rate (R_L) is:

$$R_L = \frac{e}{\varepsilon_0 \varepsilon_r} np(\mu_n + \mu_p)$$

Equation S8

Here μ is the charge mobility for electrons (n) or holes (p) as indicated by the subscripts, n is the electron density, and p is the hole density. Notably, we see that the rate of recombination is proportional to the charge carrier mobility, as was the case for charge transport. In this simple picture, the kinetic competition between Langevin recombination and charge transport is unaffected by the charge mobility. However, the (im)balance of electron and hole mobilities and charge transport times can lead to some variations.
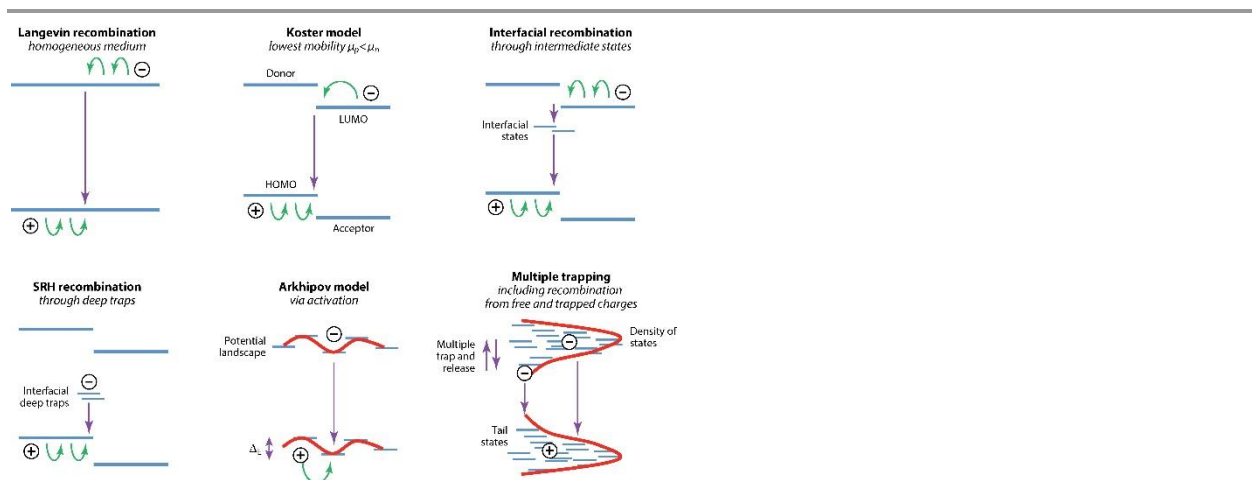

Figure S6. Overview of different types of charge recombination models. Reproduced with permission from ref [10].

In addition, a change in how charges encounter each other prior to recombination leads to a change in how mobility affects the rate of recombination.[10] For example, the Koster model[11] was proposed to explain departure from prediction of Langevin theory in polymer:fullerene solar cells. Here, the recombination rate (R_{Koster}) is dictated by the lowest charge mobility based on the argument that recombination cannot take place prior to the slowest charge reaching the interface, leading to:

$$R_{Koster} = \frac{e}{\varepsilon_0 \varepsilon_r} np \min(\mu_n, \mu_p)$$

Equation S9

Trap-assisted recombination, often called Shockley-Read-Hall (SRH) recombination, describes the recombination process of one deeply trapped and immobile charge carrier with an opposite mobile charge carrier.[12] The rate of SRH recombination is typically described in terms of capture cross-sections and the occupation probability of energetic trap states.[13] There is also some evidence that SRH capture coefficients show a Langevin-like mobility dependence,[14] resulting in:

$$R_{SRH} = \frac{e}{\varepsilon_0 \varepsilon_r} cN_t \mu_c$$

Equation S10

Here c represents the concentration of the mobile carrier, N_t the trap density, and μ_c is the mobility of the mobile carrier. Charge trapping is commonplace in semiconductors used in solar energy conversion and is thought to results in an equilibrium between trapped and free charges. The movement of charges can then be described by a multiple trapping model, where trapped charges thermally activate to a mobility edge to sample different trap states.[15] In the example of trapped holes, the recombination rate is consistent with:

$$R_{MT} = \frac{e}{\varepsilon_0 \varepsilon_r} np_{free}(\mu_n + \mu_p)$$

Equation S11

It is often intractable to experimentally determine the dominant recombination pathway, and a combination of pathways seems likely in most cases. As a result, the impact of the charge mobility on the kinetic competition between charge transport and bimolecular recombination is ill-defined yet is a key parameter for efficient device operation.[16-18]

S2.3 Charge extraction

Finally, interfacial transfer takes place leading to charge extraction from the device. A clear distinction between PV and PS is made here. For PV much care is taken to make ohmic contacts between the semiconductor and charge transport layer, keeping the energetic barrier for charge transfer to a minimum, and leading to fast charge transfer on timescales ~ nanoseconds - microseconds.[19, 20] In PS, there is often a considerable energetic barrier to the reactions that typically involve a multi-electron, multi-proton transfer. For example, water oxidation requires the proton-coupled transfer of 4 oxidative equivalents. As a result, the best performing electrocatalysis operate at an overpotential ~ 0.3 V[21-26] for charge densities of 10 mA/cm^2. Kinetically, the complexity of the reaction limits the rate of water oxidation. The typical water oxidation lifetime been determined to on the order of a few to hundreds of milliseconds for metal oxide photoanodes.[27, 28] In comparison, the oxygen-evolving complex (OEC) of PSII has a turnover frequency that equates to kinetics of roughly 2 ms.[29] The slow rate of charge extraction in PS imposes a dramatic reduction of the recombination rates for favourable kinetic competition.

To reduce the recombination at the interfaces, a common strategy has been to reduce the concentration of the opposite charge carrier. For example, this has been demonstrated through the use of rectifying interfaces[6, 30] or heterojunctions to spatially separate charge carriers, or the formation of a SCL with the associated band bending leading to the accumulation of only one type of carrier.[31-33] The increase in rate of product formation in the presence of a sacrificial reagent is also related to depletion of one type of charge carrier at the semiconductor/electrolyte interface as a result of the fast charge extraction kinetics of the sacrificial reagent.[34, 35]

S2.4 Thermodynamic limits

The thermodynamic limits have been previously discussed for solar cell devices.[36, 37] Since the mechanism of energy conversion is not taken into consideration, the same considerations are expected to be at play in PS devices. Loss processes in can be grouped into two categories: 1) extrinsic losses that are avoidable and 2) intrinsic losses that are unavoidable and are included in the theoretical efficiencies. With the focus of the present review on energetics considerations, we are mainly interested in the factors which will reduce e.g., the V$_{oc}$ of a solar cell. Thermalization is trivial in this regard: photons with energy higher than E$_g$ will quickly relax to the band edges with the excess energy released as heat.

Two other intrinsic factors reduce the V$_{oc}$ compared to the E$_g$.[37] First, the Carnot loss represents heat loss to the surroundings due to the temperature difference between the absorbing solar cell (T$_{sc}$) and the emitting Sun (T$_s$).[38] This loss is equal to $E_g \frac{T_{sc}}{T_S} \approx E_g \frac{300\ K}{5800\ K} \approx 5\%$ of E$_g$. Assuming an operating cell temperature of 100 °C, the result is still similar at $\approx 6\%$ of E$_g$. Second, the Boltzmann loss is a result of the unequal absorption and emission angles that results in entropy generation.[36] The Boltzmann loss is equal to $k_b T_{sc} \ln\left(\frac{\Omega_{sc}}{\Omega_s}\right)$ where Ω is the solid angle of the incoming sunlight (s subscript; 6.85 x 10^{-5} steradian) and emission from the solar cell (sc subscript; π steradian for a Lambertian surface). This factor is approximately 275 meV for a typical planar solar cell. Together, the Carnot and Boltzmann losses place a lower limit on ΔG$_{loss}$ of roughly 325 meV. We use this value as a rule of thumb to evaluate the energetic efficiency (through ΔG$_{loss}$) of different solar energy conversion devices.

The discrepancy between theoretical limits and state-of-the-art cells thus originates from imperfect characteristics. These include absorbing mirror back contacts, contact shadowing, high series resistance, energy offsets, charge trapping, and recombination.

S2.5 Surface recombination

For most high performance (inorganic) solar cells, extrinsic V$_{OC}$ losses arise from non-radiative surface recombination.[39, 40] To better understand the factors at play in determining V$_{OC}$, we first introduce the quasi Fermi levels:[41]

Supporting information

$$n = n_i \exp\left[\frac{q(V - \varphi_n)}{k_B T}\right]$$

Equation S12

$$p = n_i \exp\left[\frac{q(\varphi_p - V)}{k_B T}\right]$$

Equation S13

n (p) is the electron (hole) density, n_i the intrinsic carrier density, qV the energy level, and $q\varphi_{n\ (p)}$ the quasi-Fermi level of electrons (holes). V_{oc} is determined by the quasi-Fermi splitting between electrons and holes induced by light input.

$$V_{OC} = \varphi_p - \varphi_n$$

Equation S14

Combining with Equation S12 and Equation S13 above and assuming equal generation of electrons and hole under illumination (i.e., n = p), we obtain:

$$np = n^2 = n_i^2 \exp\left(\frac{qV_{OC}}{k_B T}\right)$$

Equation S15

From Equation S15 it is clear that to increase V_{OC} higher charge carrier densities need to be attained. Surface recombination is the leading process which limits charge carrier density and thus V_{OC}.[42] In fact, one can calculate the limiting V_{OC} based on the surface recombination current, as shown for Si (Figure S7).[43] A thinner Si absorber layer is more sensitive to surface recombination limitations, as expected for the higher surface/volume ratio.
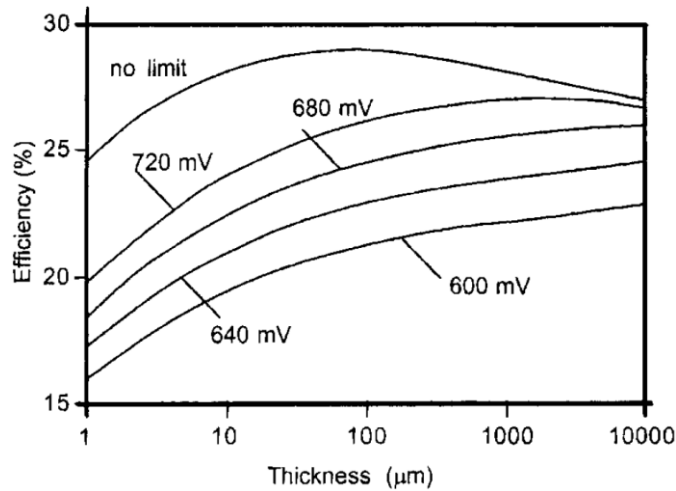

Figure S7. Calculated Si solar cell efficiency limits for different solar cell thickness. Surface recombination-limited V_{OC}'s are indicated on the curves. Reproduced with permission from ref. [43].

Recombination is often promoted at surfaces and grain boundaries due to the formation of defects.[44, 45] These can be intrinsic (e.g., dangling bonds, lattice mismatch) or extrinsic and dependant on material processing (e.g., dislocations, chemical residues, and metallic depositions). It has long been recognized that surface recombination plays a key role in determining the charge carrier lifetime in an absorber layer.[46] To reduce the density of recombination sites, different approaches are taken to reduce the density of surface recombination sites. Chemical surface passivation usually involves the growth of an (epitaxial) overlayer or addition of surface ligands.[39, 47-52] These remove defects such as under-coordinated atoms or dangling bonds. Surface modification can also induce field-effect passivation.[53] The electric fields

associated with band bending at the interface reduces the concentration of one of the carriers, slowing down recombination.

References

1. J. B. Baxter, C. Richter and C. A. Schmuttenmaer, *Annu. Rev. Phys. Chem.*, 2014, **65**, 423-447.
2. J. N. Clifford, E. Palomares, M. K. Nazeeruddin, M. Grätzel, J. Nelson, X. Li, N. J. Long and J. R. Durrant, *J. Am. Chem. Soc.*, 2004, **126**, 5225-5233.
3. S. A. Haque, S. Handa, K. Peter, E. Palomares, M. Thelakkat and J. R. Durrant, *Angew. Chem. Int. Ed.*, 2005, **44**, 5740-5744.
4. L. Wang, M. Cai, W. Sun, L. He and X. Zhang, *Adv. Mater. Interfaces*, 2018, **5**.
5. G. Liu, K. Du, S. Haussener and K. Wang, *ChemSusChem*, 2016, **9**, 2878-2904.
6. A. Reynal, J. Willkomm, N. M. Muresan, F. Lakadamyali, M. Planells, E. Reisner and J. R. Durrant, *Chem. Commun.*, 2014, **50**, 12768-12771.
7. W. Alexander, *J. Phys.: Condens. Matter*, 2017, **29**, 373001.
8. V. Coropceanu, J. Cornil, D. A. da Silva Filho, Y. Olivier, R. Silbey and J.-L. Brédas, *Chem. Rev.*, 2007, **107**, 926-952.
9. P. Langevin, *Ann. Chim. Phys*, 1903, **28**, 122.
10. G. Lakhwani, A. Rao and R. H. Friend, *Annu. Rev. Phys. Chem.*, 2014, **65**, 557-581.
11. L. J. A. Koster, V. D. Mihailetchi and P. W. M. Blom, *Appl. Phys. Lett.*, 2006, **88**, 052104.
12. W. Shockley and W. T. Read, *Physical Review*, 1952, **87**, 835-842.
13. M. M. Mandoc, F. B. Kooistra, J. C. Hummelen, B. de Boer and P. W. M. Blom, *Appl. Phys. Lett.*, 2007, **91**, 263505.
14. M. Kuik, L. J. A. Koster, G. A. H. Wetzelaer and P. W. M. Blom, *Phys. Rev. Lett.*, 2011, **107**, 256805.
15. J. Nelson, *Physical Review B*, 2003, **67**, 155209.
16. S. Shoaee, M. Stolterfoht and D. Neher, *Adv. Energy Mater.*, 2017, DOI: 10.1002/aenm.201703355.
17. M. C. Heiber, T. Okubo, S.-J. Ko, B. R. Luginbuhl, N. A. Ran, M. Wang, H. Wang, M. A. Uddin, H. Y. Woo, G. C. Bazan and T.-Q. Nguyen, *Energ. Env. Sci.*, 2018, DOI: 10.1039/C8EE01559G.
18. T. Kirchartz and U. Rau, *Adv. Energy Mater.*, 2018, **8**.
19. A. Melianas, F. Etzold, T. J. Savenije, F. Laquai, O. Inganäs and M. Kemerink, *Nat. Commun.*, 2015, **6**, 8778.
20. R. Ihly, A.-M. Dowgiallo, M. Yang, P. Schulz, N. J. Stanton, O. G. Reid, A. J. Ferguson, K. Zhu, J. J. Berry and J. L. Blackburn, *Energ. Env. Sci.*, 2016, **9**, 1439-1449.
21. C. C. L. McCrory, S. Jung, J. C. Peters and T. F. Jaramillo, *Journal of the American Chemical Society*, 2013, **135**, 16977-16987.
22. N.-T. Suen, S.-F. Hung, Q. Quan, N. Zhang, Y.-J. Xu and H. M. Chen, *Chem. Soc. Rev.*, 2017, **46**, 337-365.
23. B. M. Hunter, H. B. Gray and A. M. Müller, *Chem. Rev.*, 2016, **116**, 14120-14136.
24. I. Roger, M. A. Shipman and M. D. Symes, *Nat. Rev. Chem.*, 2017, **1**, 0003.
25. M. Tahir, L. Pan, F. Idrees, X. Zhang, L. Wang, J.-J. Zou and Z. L. Wang, *Nano Energy*, 2017, **37**, 136-157.
26. C. C. McCrory, S. Jung, I. M. Ferrer, S. M. Chatman, J. C. Peters and T. F. Jaramillo, *J. Am. Chem. Soc.*, 2015, **137**, 4347-4357.
27. C. A. Mesa, L. Francas, K. R. Yang, P. Garrido-Barros, E. Pastor, Y. Ma, A. Kafizas, T. E. Rosser, M. T. Mayer, E. Reisner, M. Gratzel, V. S. Batista and J. R. Durrant, *Nat. Chem.*, 2020, **12**, 82-89.

28.   L. Francàs, C. Mesa, E. Pastor, F. Le Formal and J. R. Durrant, in *Advances in Photoelectrochemical Water Splitting: Theory, Experiment and Systems Analysis*, eds. S. D. Tilley, S. Lany and R. Van de Krol, Royal Society of Chemistry, London, 2018, DOI: 10.1039/9781782629863, ch. 5, pp. 128-162.

29.   W. Lubitz, E. J. Reijerse and J. Messinger, *Energ. Env. Sci.*, 2008, **1**, 15-31.

30.   T. J. Barr, A. J. Morris, A. Taheri and G. J. Meyer, *J. Phys. Chem. C*, 2016, **120**, 27173-27181.

31.   M. Barroso, C. A. Mesa, S. R. Pendlebury, A. J. Cowan, T. Hisatomi, K. Sivula, M. Grätzel, D. R. Klug and J. R. Durrant, *Proc. Natl. Acad. Sci. U. S. A.*, 2012, **109**, 15640-15645.

32.   S. R. Pendlebury, X. Wang, F. Le Formal, M. Cornuz, A. Kafizas, S. D. Tilley, M. Grätzel and J. R. Durrant, *Journal of the American Chemical Society*, 2014, **136**, 9854-9857.

33.   K. Appavoo, M. Liu, C. T. Black and M. Y. Sfeir, *Nano Lett.*, 2015, **15**, 1076-1082.

34.   F. E. Osterloh, *ACS Energy Lett.*, 2017, DOI: 10.1021/acsenergylett.6b00665, 445-453.

35.   Y. Pellegrin and F. Odobel, *Comptes Rendus Chimie*, 2017, **20**, 283-295.

36.   T. Markvart, *Appl. Phys. Lett.*, 2007, **91**, 064102.

37.   L. C. Hirst and N. J. Ekins-Daukes, *Progress in Photovoltaics: Research and Applications*, 2011, **19**, 286-293.

38.   P. T. Landsberg and V. Badescu, *J. Phys. D: Appl. Phys.*, 2000, **33**, 3004.

39.   A. G. Aberle, *Progress in Photovoltaics: Research and Applications*, 2000, **8**, 473-487.

40.   G. Dingemans and W. M. M. Kessels, *Journal of Vacuum Science & Technology A: Vacuum, Surfaces, and Films*, 2012, **30**, 040802.

41.   M. Rudan, in *Physics of Semiconductor Devices*, Springer International Publishing, Cham, 2018, DOI: 10.1007/978-3-319-63154-7_19, pp. 453-505.

42.   J. M. Pearce, R. J. Koval, A. S. Ferlauto, R. W. Collins, C. R. Wronski, J. Yang and S. Guha, *Appl. Phys. Lett.*, 2000, **77**, 3093-3095.

43.   M. A. Green, *Progress in Photovoltaics: Research and Applications*, 1999, **7**, 327-330.

44.   H. C. Card and E. S. Yang, *IEEE Transactions on Electron Devices*, 1977, **24**, 397-402.

45.   M. Taguchi, A. Yano, S. Tohoda, K. Matsuyama, Y. Nakamura, T. Nishiwaki, K. Fujita and E. Maruyama, *IEEE Journal of Photovoltaics*, 2014, **4**, 96-99.

46.   P. Dawson and K. Woodbridge, *Appl. Phys. Lett.*, 1984, **45**, 1227-1229.

47.   G. Dingemans, W. Beyer, M. C. M. v. d. Sanden and W. M. M. Kessels, *Appl. Phys. Lett.*, 2010, **97**, 152106.

48.   R. Godin, X. Ma, S. González-Carrero, T. Du, X. Li, C.-T. Lin, M. A. McLachlan, R. E. Galian, J. Pérez-Prieto and J. R. Durrant, *Adv. Optical Mater.*, 2018, **6**, 1701203.

49.   D. W. deQuilettes, S. Koch, S. Burke, R. K. Paranji, A. J. Shropshire, M. E. Ziffer and D. S. Ginger, *ACS Energy Lett.*, 2016, **1**, 438-444.

50.   G. Mariani, A. C. Scofield, C.-H. Hung and D. L. Huffaker, 2013, **4**, 1497.

51.   P. Reiss, M. Protière and L. Li, *Small*, 2009, **5**, 154-168.

52.   F. Le Formal, N. Tétreault, M. Cornuz, T. Moehl, M. Grätzel and K. Sivula, *Chem. Sci.*, 2011, **2**, 737-743.

53.   B. Hoex, J. J. H. Gielis, M. C. M. v. d. Sanden and W. M. M. Kessels, *J. Appl. Phys.*, 2008, **104**, 113703.